Journal of Advanced Research 20 (2019) 79–89

Contents lists available at ScienceDirect

Journal of Advanced Research

journal homepage: www.elsevier.com/locate/jare

Original article

Natural rubber/reduced-graphene oxide composite materials: Morphological and oil adsorption properties for treatment of oil spills

Siripak Songsaeng [a], Patchanita Thamyongkit [b], Sirilux Poompradub [c,d,e,*]

[a] Program in Hazardous Substance and Environmental Management, Chulalongkorn University, Bangkok 10330, Thailand
[b] Department of Chemistry, Faculty of Science, Chulalongkorn University, Bangkok 10330, Thailand
[c] Department of Chemical Technology, Faculty of Science, Chulalongkorn University, Bangkok 10330, Thailand
[d] Center of Excellence on Petrochemical and Materials Technology, Chulalongkorn University, Bangkok 10330, Thailand
[e] Green Materials for Industrial Application Research Unit, Faculty of Science, Chulalongkorn University, Bangkok 10330, Thailand

HIGHLIGHTS

- Natural rubber/rGO composite foam was used as an oil sorbent.
- Addition of rGO enhanced the oil adsorption capacity and strength of NR sorbent foam.
- Inclusion of 0.5 phr rGO into NR increased the crude oil adsorption capacity to 17.04 g g^{-1}.
- Oil adsorption mechanism of the sorbent materials was proposed.
- Reusability of the NR/rGO sorbent was greater than 70% oil adsorption for 30 cycles.

GRAPHICAL ABSTRACT

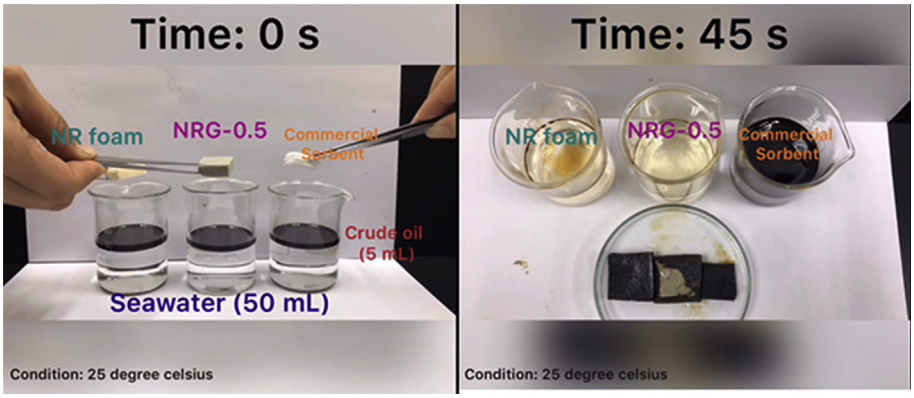

ARTICLE INFO

Article history:
Received 22 February 2019
Revised 7 May 2019
Accepted 30 May 2019
Available online 31 May 2019

Keywords:
Oil sorbent
Natural rubber
Reduced graphene oxide
Composite material
Adsorption isotherm
Reusability

ABSTRACT

A green sorbent material was fabricated through the simple addition of reduced graphene oxide (rGO) to natural rubber (NR) latex. The effect of rGO content in the NR foam on petroleum oil adsorption was investigated. The addition of rGO in NR increased the petroleum oil adsorption capacity of the resulting NR/rGO (NRG) composite foam (12–21 g g^{-1}) with respect to those of the pure NR foam (8–15 g g^{-1}) and a commercial sorbent (6–7 g g^{-1}). The adsorption capacity was optimal for 0.5 phr rGO (NRG-0.5). Further, the environmental conditions (temperature and waves) affected the oil adsorption capacity of the sorbent materials. The adsorption kinetics of the sorbent materials for crude AXL oil was best described with pseudo-second-order kinetics. The interparticle diffusion model revealed three steps whereas the adsorption isotherms approximated the Langmuir isotherms. Moreover, the oil adsorption mechanisms of the NR and NRG sorbent materials were compared to that of a commercial sorbent. The high elasticity of the NRG-0.5 composite foam improved not only the oil adsorption capacity but also the reusability of the sorbent material. The presence of rGO increased the strength of the NRG-0.5 compared to that of pure NR, which resulted in a high-performance and reusable material with an oil removal efficiency higher than 70% after 30 uses.

Peer review under responsibility of Cairo University.

* Corresponding author.
E-mail address: sirilux.p@chula.ac.th (S. Poompradub).

https://doi.org/10.1016/j.jare.2019.05.007
2090-1232/

Introduction

Since the industrial revolution, the demand for petroleum products has remarkably increased, thereby leading to an increased risk and frequencies of oil leakages through the extraction, transportation, transfer, and storage of oil. Oil spills in the natural environment cause catastrophic effects on the environment and ecosystem [1–3]. Various methods have been developed to solve this serious problem, such as physical [4–7], chemical [8–10], and biological [11–13] approaches. The physical adsorption by an adsorbent is considered to be an efficient technique for the treatment of oil spills because it is simple, environmentally friendly, and requires low costs. The method involves using a sorbent to collect and transform the liquid oil into a semi-solid or solid phase that can be easily removed from the contaminated site. Generally, sorbent materials can be classified into three groups: synthetic materials [14–16], inorganic minerals [17–19], and natural products [20–23].

Currently, three-dimensional hydrophobic and oleophilic porous materials are popular candidates for the oil absorption of spills because of their suitable selectivities for oil and organic solvents, high absorption capacities, and excellent reusability and oil recovery. However, most reported studies have focused on synthetic materials, such as polyurethane foam [14–16], poly(tetrahydrofuran) [3], and polydimethylsiloxane sponges [24–27]. The disadvantages of these synthetic sorbents are their high production costs and large waste volumes. Although polystyrene [28,29] is cheap and lightweight, it burns easily and produces toxic combustion fume. Thus, natural rubber (NR) is a more interesting alternative.

Natural rubber (NR) is an important renewable polymeric material with outstanding flexibility and excellent mechanical properties. It can be easily produced as NR foam, which has a high porosity, low density, and strong hydrophobic property [30,31]. Therefore, NR foams are good candidates as oil sorbent materials. Several techniques have been studied to improve the oil adsorption capacity of NR foams, including chemical modifications [32,33] and the preparation of composite materials [26,34–37].

In this study, reduced graphene oxide (rGO) was added to NR to improve its oil adsorption capacity because the chemical rGO structure is similar to that of graphene and it has a high surface area and tensile strength [2,38,39]. Further, it causes fewer costs than graphene. Additionally, rGO is compatible with the NR matrix owing to its hydrophobic property, which enables a more homogenously mixed phase. To create the green composite material, rGO was synthesized from graphite waste obtained from a metal smelting company. Based on the previous study presented in [40], rGO was prepared by the Hummer's method. The rGO was used to improve the conductivity and mechanical properties of the NR vulcanizates. Therefore, its functions were investigated in the present study. The focus of this study was to design and prepare a novel NR/rGO (NRG) oil adsorption composite. The high elasticity of the NR and the highly active surface area of the rGO led to an enhanced oil absorptivity and stability of the composite under working conditions. The sorption mechanisms were intensively investigated to determine the factors that affect the oil sorption performance of the composite. The results of this extensive study might provide useful guidelines for the further development and exploitation of NR for environmental conservation purposes.

More specifically, the aim of this research study was to study the influence of the rGO content on the oil adsorption capacity of an NRG foam composite material with respect to the properties of pure NR foam and commercial polypropylene sorbent pads (CM). The relationship between the morphology and adsorption capacity of the different sorbent materials was investigated. Further, the effects of the temperature and waves on the oil adsorption capacity of each sorbent material were examined for their applications in real oil spill removals in marine environments. The kinetics and adsorption isotherms of the obtained sorbent materials were evaluated and their oil adsorption mechanisms proposed. Finally, the reusability of the selected NRG sorbent was examined in comparison to that of the CM sorbent.

Material and methods

Materials

The graphite waste was obtained from a local metal smelting company (Mahamek Flow Innovation Co., Ltd., Bangkok, Thailand), and the sulfuric acid (98% (*w/v*); H_2SO_4), potassium permanganate ($KMnO_4$), hydrochloric acid (36% (*w/v*); HCl), and L-ascorbic acid (L-AA) were purchased from QREC Chemical Ltd. (Chonburi, Thailand). The sodium hydroxide (NaOH) was purchased from Ajax Finechem Ltd. (Auckland, New Zealand). Further, the high-ammonia NR latex (60% dry rubber content) and following curing agents: 10% potassium oleate (K-oleate) dispersion, 50% sulfur dispersion, 50% zinc diethyldithiocarbamate (ZDEC) dispersion, 50% zinc-2-mercaptobenzothiazole (ZMBT) dispersion, 50% Wingstay®-L, 33% dipropylene glycol (DPG) dispersion, 50% zinc oxide (ZnO) dispersion, and 12.5% sodium silicofluoride (SSF) dispersion originate from the Rubber Research Institute, Bangkok, Thailand. The gasoline (density of 0.74 g/cm^3 and viscosity of 1.42 mPa) and crude AXL oil (density of 0.84 g/cm^3 and viscosity of 3.80 mPa) were purchased from PTT Public Co., Ltd., and Thai Oil PCL Ltd., Bangkok, Thailand, respectively. The commercial polypropylene sorbent pad (CM) originates from Surface Pro-Tech Co., Ltd. (Chonburi, Thailand).

Synthesis of rGO

The procedure for the rGO synthesis was performed according to the modified Hummer's method [37] and was followed by a reduction with L-AA [38,41,42]. The graphite waste (3 g) was added to 60 mL concentrated H_2SO_4 under agitation in an ice bath at 10 °C. Then, $KMnO_4$ (9 g) was slowly added, followed by the careful addition of 150 mL deionized water under stirring and heating to 95 °C for 15 min before an ultrasonic treatment at room temperature for 30 min. The mixture was then adjusted to pH 8–9 through the addition of 1 M NaOH solution, whereupon 0.5 M L-AA was added to the colloidal solution. The reaction was stirred at 95 °C for 1 h. The resultant black precipitate was filtered through Whatman (No. 40) filer paper, washed with 1.0 M HCl and then deionized water until the filtrated water exhibited a pH value of 7. The final product (rGO) was dried in an oven at 100 °C for 24 h.

Characterization of rGO

Raman spectroscopy was conducted with a DXR Raman microscope (Thermo Fisher Scientific, Massachusetts, USA). A 780 nm laser was used as light source with a spot size of approximately 3 μm. The Raman spectra were recorded from 800 to 1800 cm^{-1}.

Further, water contact angle measurements were carried out with a ramé-hart instrument (New Jersey, USA) at ambient temperature. The powder sample was pasted onto a glass slide with an adhesive tape. The water contact angle was measured by placing a 50 μL deionized-water droplet onto the sample surface with a micro-syringe. Each sample was measured from five different positions and evaluated with the averaged values.

The morphologies of the graphite, graphite oxide (GO), and rGO were examined by transmission electron microscopy (TEM) (TECNAI 20, Philips, Oregon, USA). A sample (0.1 g) in absolute ethanol was sonicated in a sonication bath for 15 min followed by a vortex

treatment for 5 min. Afterward, the colloidal solution was dropped onto the TEM grid.

Preparation of NR and NRG sorbent materials

The formulations for the NR and different NRG-X (where X is the rGO content in parts by weight per hundred parts of rubber; phr) foam sorbents used in this study are shown in Table 1. The NR latex and all curing agents were mixed in a cake mixer at room temperature, compounded with the desired amount of rGO (0, 0.25, 0.5, 1, and 1.5 phr), quickly poured into an aluminum mold, and vulcanized at 100 °C for 2 h. The vulcanized NR and NRG-X foams were then washed with water to remove unreacted elements. Finally, they were dried in an oven at 60 °C for 24 h.

Characterization of sorbent materials

The morphologies of the sorbent materials were characterized by scanning electron microscopy (SEM) (JEOL JSM-6480LV; Tokyo, Japan) at an acceleration voltage of 10 kV. The sorbent materials were cut and stitched onto an SEM stub and coated with gold before the SEM analysis.

The surface wettabilities of the sorbent materials were measured by dropping 0.1 mL of water, seawater, and crude oil onto each sorbent surface at room temperature. The digital images of the liquid droplets were recorded at a magnification of 2.5.

Dynamic mechanical properties of NR composite foam were examined by dynamic mechanical analyzer (DMA, GABO, model EPLEXOR QC 100, Ahlden, Germany). The sample size was 8 mm × 8 mm × 4 mm. The tensile mode was used at a frequency of 10 *Hz*, a static strain of 1.0% and a dynamic strain of 0.1%. The temperature was in the range of −100 °C to 80 °C with a heating rate of 2 °C/min.

Determination of oil sorption capacity

The method for the determination of the oil adsorption capacity was based on the standard test method for the adsorbent performance (ASTM F726-12). The oil sorption experiment was conducted by pouring 3 g oil into 100 mL water or seawater. The sorbent materials were cut into cubes ($0.7 \times 0.7 \times 0.7\ cm^3$) and weighed before their immersion into the oil–water or oil–seawater systems. After 15 min, the sorbents were removed from the systems. The excess oil on the sorbent surface was removed, and the sorbents were weighed. The effects of the temperature (4–70 °C) and waves (0–200 revolutions per minute: rpm) were investigated. The waves were generated by a shaker (VS-202P, Vision Scientific Co., Ltd., Korea) at room temperature. The sorption capacity (%) was calculated with Eq. (1) [43]:

$$Q(g \cdot g^{-1}) = \frac{(W_1 - W_0)}{W_0}, \quad (1)$$

where Q is the oil adsorption capacity (g g^{-1}), and W_0 and W_1 represent the initial weight and weight of the foam after the adsorption, respectively.

To assess the reusability of the sorbents, the oil was removed from the saturated sorbent by squeezing. Next, the sorbent was weighed and immersed again into the oil–seawater system. This adsorption–desorption cycle was performed for up to 30 cycles to determine the oil removal efficiency (Re) [32]:

$$Re(\%) = \frac{(W_1 - W_0)}{W_1} \times 100. \quad (2)$$

Kinetic and isotherm studies

The pseudo-first-order, pseudo-second-order, and intraparticle diffusion models are expressed in Eqs. (3)–(5) [44–47]:

$$\text{Pseudo} - \text{first} - \text{order model}: \quad \ln(Q_e - Q_t) = \ln Q_e - k_1 t, \quad (3)$$

$$\text{Pseudo} - \text{second} - \text{order model}: \quad \frac{t}{Q_t} = \frac{1}{k_2 Q_e^2} + \frac{1}{Q_e}, \quad (4)$$

$$\text{Intraparticle model}: \quad Q_t = k_d t^{1/2}, \quad (5)$$

where Q_t and Q_e are the amounts of adsorbate (g g^{-1}) at time (t) and equilibrium, respectively; k_1 (min^{-1}) is the pseudo-first-order rate constant, k_2 (g g^{-1} min^{-1}) is the pseudo-second-order rate constant, and k_d is the intraparticle diffusion rate constant (g g^{-1} $s^{1/2}$).

The adsorption isotherm was calculated with the Langmuir and Freundlich models based on Eqs. (6) and (7) to estimate the maximal amount of adsorbed oil [47–49]:

$$\frac{C_e}{Q_e} = \frac{1}{Q_m k_L} + \frac{C_e}{Q_m}, \text{ where } R_L = \frac{1}{1 + k_L C_o} \quad (6)$$

$$\ln Q_e = \ln k_F + \frac{1}{n} \ln C_e \quad (7)$$

where Q_m and Q_e are the maximal adsorption capacity (g g^{-1}) and the amount of adsorbed oil at equilibrium, respectively; C_e (g L^{-1}) is the oil concentration at equilibrium, and k_L (L g^{-1}) is the Langmuir constant that is related to the adsorption energy. An important characteristic of the Langmuir isotherm is the separation factor (R_L), which expresses the adsorption nature as irreversible ($R_L = 0$),

Table 1
Formulation of NR foam and NRG-X composite foams.

Reagent	Dry weight (phr[a])				
	NR	NRG-0.25	NRG-0.5	NRG-1.0	NRG-1.5
NR Latex (60% DRC[b])	100.00	100.00	100.00	100.00	100.00
10% K-oleate	1.50	1.50	1.50	1.50	1.50
50% Sulfur dispersion	2.00	2.00	2.00	2.00	2.00
50% ZDEC	1.00	1.00	1.00	1.00	1.00
50% ZMBT	1.00	1.00	1.00	1.00	1.00
50% Wingstay®L dispersion	1.00	1.00	1.00	1.00	1.00
33% DPG	0.66	0.66	0.66	0.66	0.66
50% ZnO	5.00	5.00	5.00	5.00	5.00
12.5% SSF	1.00	1.00	1.00	1.00	1.00
rGO	–	0.25	0.50	1.00	1.50

[a] Parts by weight per hundred parts of rubber.
[b] Dry rubber content.

favorable ($0 < R_L < 1$), linear ($R_L = 1$), or unfavorable ($R_L > 1$) [49]; C_o (g L^{-1}) is the initial oil concentration. The term k_F (g g^{-1}) is the Freundlich constant related to the adsorption capacity. The slope *1/n* describes the adsorption intensity or surface heterogeneity [47].

Results and discussion

Textural properties of rGO

The Raman spectra of the graphite, GO, and rGO are shown in Fig. 1. The Raman spectrum of graphite exhibits a strong G band at 1580 cm^{-1}, which is related to the in-plane vibrations of the sp^2-hybridized carbon atoms [50,51]. The weak D band corresponding to the presence of vacancies or dislocations in the graphene layer and at the edges is approximately located at 1300 cm^{-1} [51,52]. The Raman spectra of GO and rGO exhibit broad G and D (with high intensities) bands owing to the disordered arrangements of the carbon planes.

The TEM image (Fig. 2) of the graphite displays a dark flake due to the stacking of multi-layer graphene sheets through van der Waal forces. The GO structure was more transparent and consisted of few-layer sheets after the oxidation process. The oxygen-containing groups destroyed the van der Waal interactions among the graphene sheets of the GO structure. Thus, the graphene sheets were easily separated by the exfoliation step. After the reduction, the transparent rGO had few thin sheets with typical wrinkled and scrolled structures.

A high contact angle was obtained for graphite (151°), as shown in Fig. 2, whereas that of rGO tended to decrease (133°) owing to the different surface wettability of the graphite after the chemical treatment through the modified Hummer's method. Unfortunately, the wettability measurements could not be conducted for the GO sample owing to its high hydrophobicity originating from the oxygen-containing groups in the GO.

Morphologies of sorbent materials

The SEM images of each sorbent material are shown in Fig. 3. The morphologies of the NR and different NRG-X sorbent materials exhibited open-cell structures with spherical shapes. Each cell structure consisted of pores of various sizes. The cell sizes of the NRG-X composite materials tended to increase with increasing rGO content owing to the rGO interference during the foaming process. The aggregation or agglomeration of rGO particles was evident (inset in Fig. 3) and became more evident with increasing rGO content. This result implies that the aggregation/agglomeration of rGO particles might affect not only the formation of the cell structure but also the composite properties in terms of mechanical,

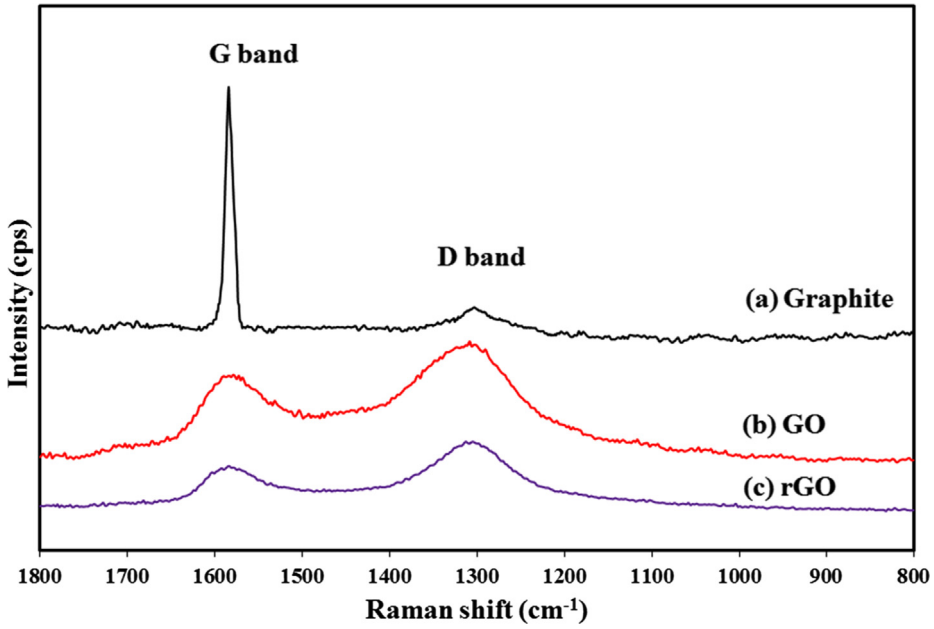

Fig. 1. Raman spectra of (a) graphite, (b) GO, and (c) rGO.

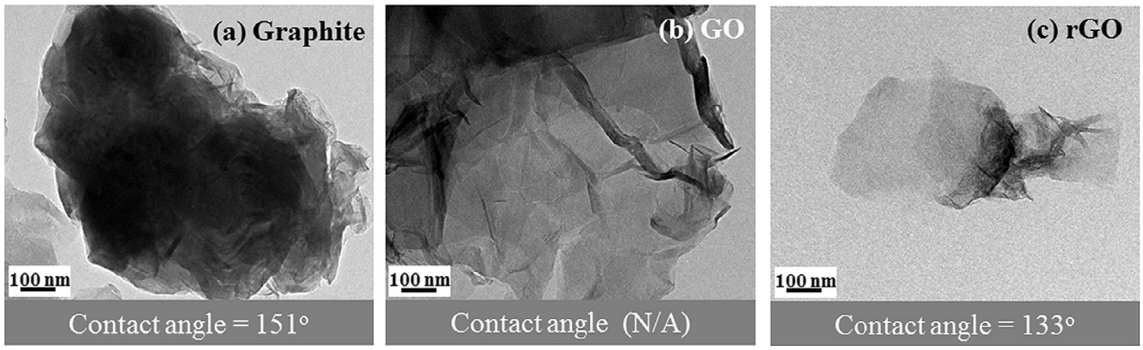

Fig. 2. TEM images and contact angles of (a) graphite, (b) GO, and (c) rGO.

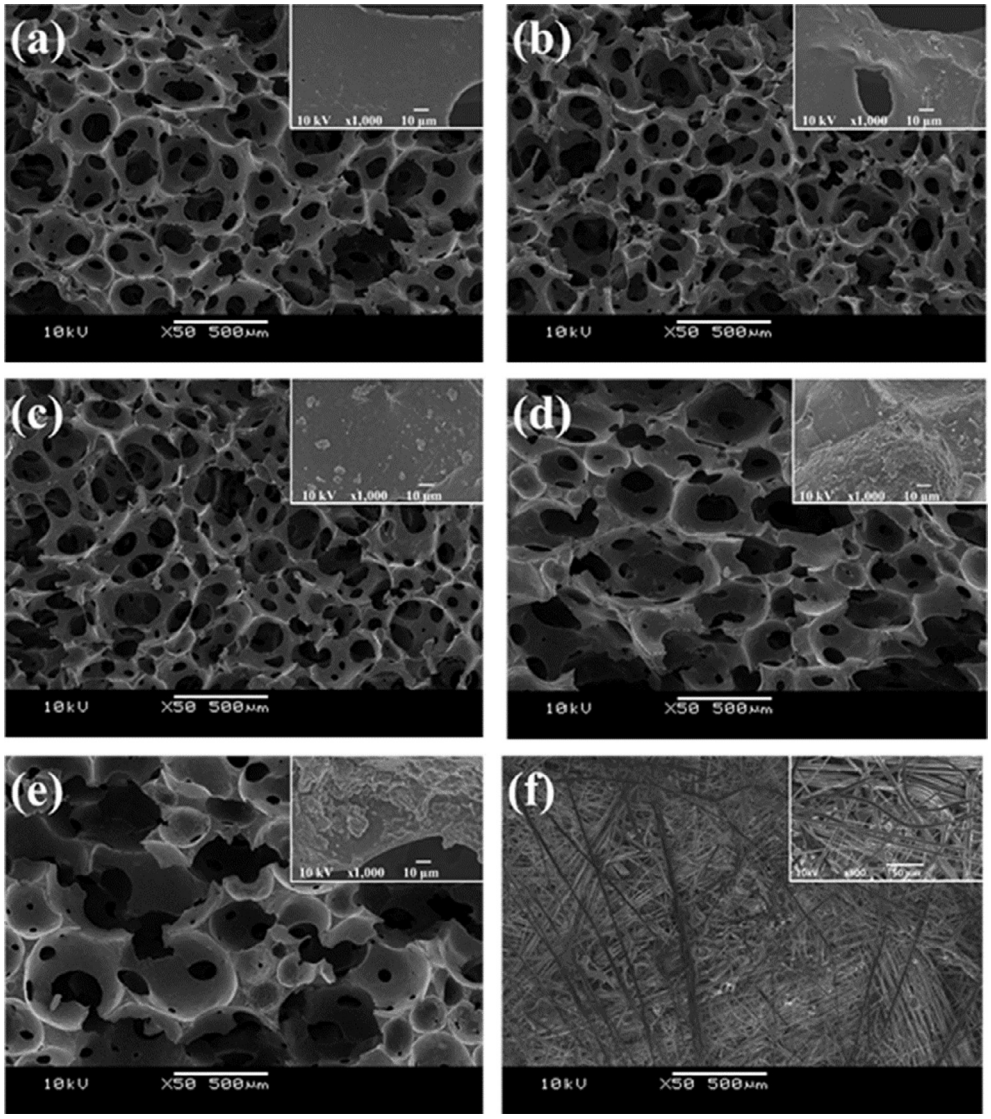

Fig. 3. SEM images (50× magnification) of (a) NR, (b) NRG-0.25, (c) NRG-0.5, (d) NRG-1.0, (e) NRG-1.5, and (f) CM sorbents.

thermal, physical, or electrical properties [40]. By contrast, the CM sorbent exhibited an entangled fibrous structure of various sizes.

Surface and viscoelastic properties of sorbent materials

Fig. 4 compares the surface wettabilities of the sorbent materials for water, seawater, and crude AXL oil on the sorbent surfaces. Each sorbate exhibited a different behavior during the adsorption process. Among the three sorbent materials (NR, NRG-0.5, and CM), the water or seawater droplet was more stable (with a half-spherical shape and contact angle of 124°) on the CM, which implies that the surface of the CM sorbent was more hydrophobic. However, the hydrophobicities of the NR and NRG-0.5 sorbents tended to decrease, as indicated by the decreased contact angles (74° and 83°, respectively). Further, the water and seawater droplet shapes became oval. Owing to the insignificant difference between the water contact angles of NR and NRG-0.5, it can be concluded that the added rGO in the NR was compatible with the NR surface. However, the surfaces of NR and NRG-0.5 were highly porous. The sorbate (water or seawater) could penetrate into the pores, thereby resulting in a decreased contact angle. Accordingly, these three sorbent materials could adsorb the crude oil well. The adsorption of highly viscous oil causes the formation of a shear layer of large volume across the sorbent surface. The dispersion of crude oil on the CM surface during the adsorption led to a larger coverage compared with those on the NR and NRG-0.5 sorbent materials. This was due to the different morphologies of the sorbents. Regarding the CM, the diffused oil traveled along the fiber length, whereas those of the NR and NRG-0.5 sorbents penetrated the pores. The dynamic mechanical properties of NR composite foams were shown in Fig. 5. The presence of rGO in the rubbery matrix did not affect the viscoelastic properties in terms of the storage modulus (E′) and tan δ, due to dilution effect of rGO.

Adsorption abilities of sorbent materials

Oil adsorption

The adsorption performances of the sorbent materials for different aqueous media are shown in Fig. 6. Two types of oil (gasoline and crude AXL oil) were used as representatives of a petroleum oil leakage. In the oil–water system (Fig. 6(a)), the oil adsorption capacity of the NRG-X composite foams was higher (1.2–1.36 times and 1.5–1.98 times for gasoline and crude oil, respectively) than that of the NR foam. This was because the rGO content in the NR

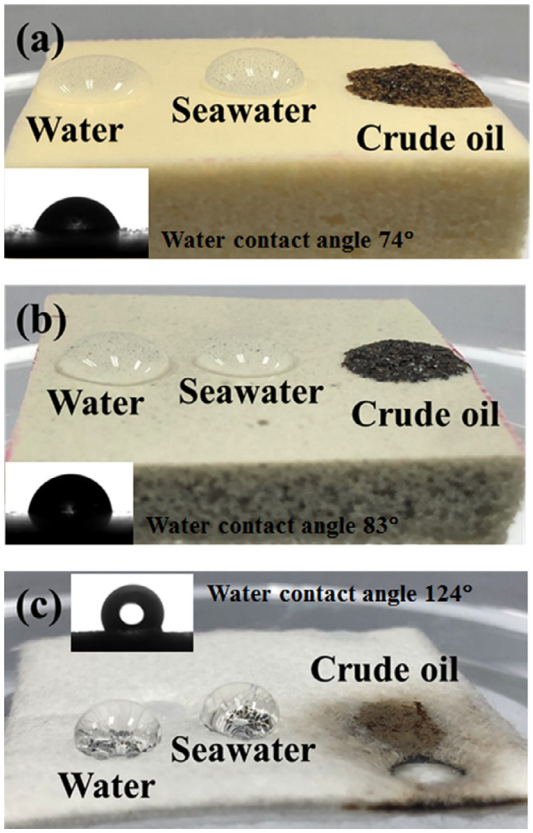

Fig. 4. Images of surface wettabilities of (a) NR, (b) NRG-0.5, and (c) CM sorbents for sorbate droplets of 0.1 mL water, seawater, and crude AXL oil.

foam created an increased surface area for the sorbent materials, thereby resulting in an enhanced oil adsorption. The oil adsorption increased with increasing rGO levels up to 0.5 phr. However, the addition of more than 0.5 phr rGO in the NR foam decreased the oil adsorption capacity because the petroleum oil could not be retained in the large pores of the sorbent matrix, as discussed in the previous section.

In the oil–seawater system (Fig. 6(b)), the oil adsorption of the sorbent materials was slightly (<1.2-fold) higher than that in the oil–water system, which was due to the effect of salinity, ions, and foreign matter. The salinity in seawater can increase the electrical double layer between the sorbate and sorbent materials, thereby leading to an increased oil adsorption capacity [53]. The maximal oil adsorption performance was obtained with NRG-0.5. Thus, the NRG-0.5 sorbent was selected for further studies.

Furthermore, the oil adsorption capacity depended on the density and viscosity of the oil. The lowly viscous oil (gasoline) could easily diffuse on the surface and immediately penetrate the sorbent pores, whereas the highly viscous oil (crude AXL oil) remained at the sorbent surface and retarded the oil penetration into the interior pore structure. Accordingly, the sorbent materials swelled more rapidly with a lowly viscous oil than with a highly viscous oil.

The oil adsorption capacities of the CM, NR, and NRG-0.5 sorbents were evaluated for constant weights and volumes (0.05 g and 0.34 cm^3). The oil adsorption capacity of the CM sorbent in the oil–water or oil–seawater systems was remarkably lower (30–40%) than those of the NR and NRG-0.5 sorbents. Moreover, the effect of the oil viscosity on the adsorption performance of the CM did not change noticeably. This was due to the different morphological structures of CM compared with those of the NR and NRG-0.5 sorbents.

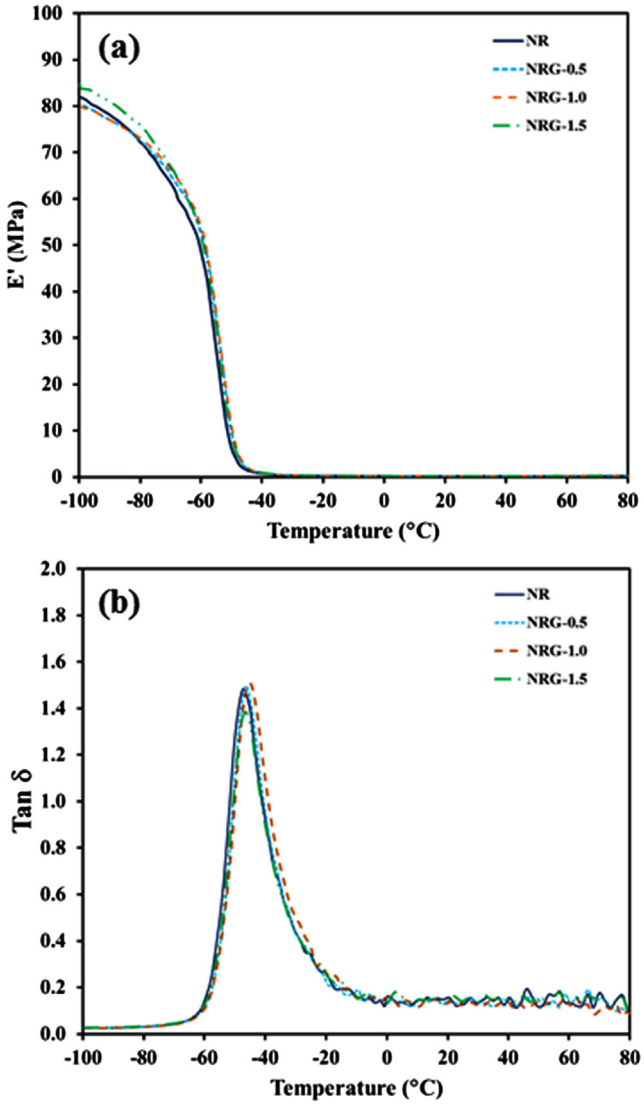

Fig. 5. (a) Storage modulus (E′) and (b) Tan δ versus temperature of NR composite foams.

Effect of environmental conditions

The application of these sorbent materials to a marine oil spill situation was the main objective of this study. Accordingly, the effects of environmental marine conditions (temperature and waves) on the adsorption capacities for crude AXL oil of the different sorbent materials (NR, NRG-0.5, and CM) were examined. The results are presented in Fig. 7. When the temperature increased from 4 to 45 °C and 100 rpm waves were created, the oil adsorption capacities of the NR and NRG-0.5 sorbents increased 3 and 2.4 times, respectively. However, they decreased at higher temperatures (60 and 70 °C) with a maximal capacity at 45 °C (Fig. 7(a)). The temperature is a main factor affecting the oil adsorption capacities of the sorbent materials because it changes the oil viscosity [54–57]. Generally, the viscosity of a material decreases with increasing temperature. However, in addition to the temperature effect, the increasing temperatures cause an NR and NRG-0.5 sorbent shrinkage owing to the elastomeric behavior. This could explain why the oil adsorption capacities of the NR and NRG-0.5 sorbents decreased above 45 °C. As the rubber chains shrank at higher temperatures, the retention of the oil in the rubber pores decreased. This behavior was not observed for the CM sorbent

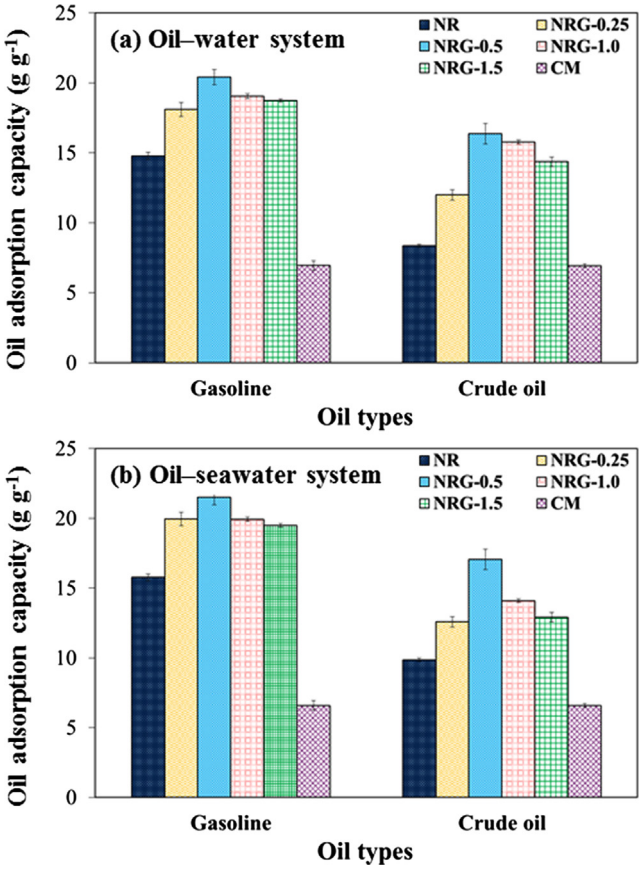

Fig. 6. Oil adsorption capacities of sorbent materials in (a) oil–deionized water and (b) oil–seawater systems.

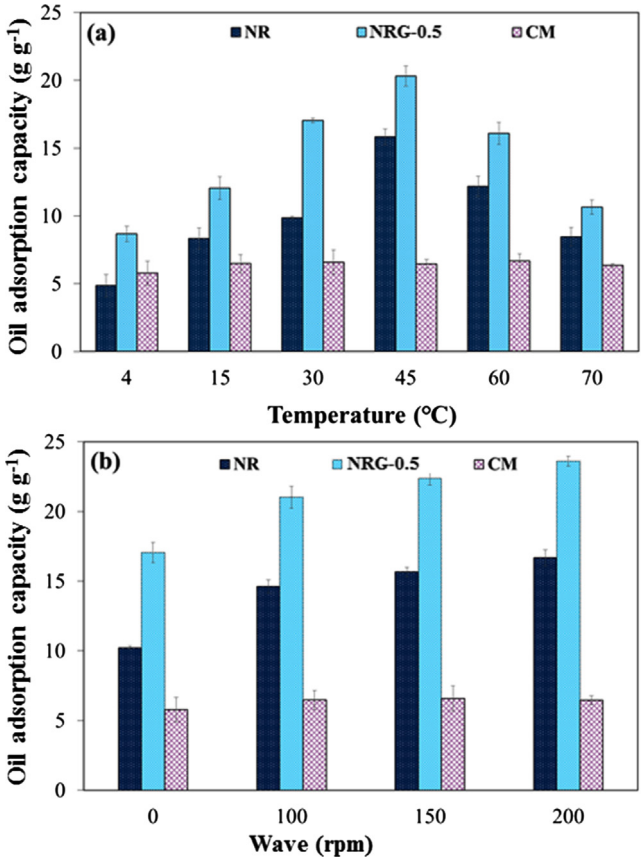

Fig. 7. Effect of environmental conditions: (a) with respect to temperature and 100 rpm waves and (b) waves at a temperature of 45 °C on the adsorption capacities of the sorbent materials for crude AXL oil.

owing to the different thermal properties of the NR elastomer and polypropylene plastic.

The effect of the waves on the oil adsorption capacities of the NR, NRG-0.5, and CM sorbents at 45 °C is shown in Fig. 7(b). When the waves were introduced with a shaker, the oil adsorption capacities of the NR and NRG-0.5 sorbents gradually increased with increasing waves; they were 1.6 and 1.4 higher at 200 rpm than at 0 rpm, respectively. The enhanced oil adsorption capacities were due to the external force applied by the waves, which resulted in an increased oil diffusion into the sorbent matrix. By contrast, the oil adsorption capacity of CM under different waves remained essentially constant owing to the limitation of the oil diffusion along the fiber length. In addition, all sorbents continued to float on the seawater surface after the complete saturation, thereby illustrating their good buoyancies. Therefore, the NR and NRG-0.5 sorbents can potentially be used as petroleum oil sorbents in real oil spill situations.

Adsorption kinetics and isotherm studies

In this study, the pseudo-first-order and pseudo-second-order rate equations were used to study the kinetic adsorption of the sorbent materials for crude AXL oil. The results are summarized in Table 2. The data of all three sorbent materials approximated the pseudo-second-order model with a correlation coefficient (R^2) of approximately 1 (0.99). In addition, the $Q_{e,cal}$ values of the three sorbent materials were approximately comparable to the experimental value ($Q_{e,\exp}$). The highest oil adsorption rate (k_2) was obtained for NRG-0.5 because the presence of rGO in the composite foam increased the sorbent surface area and thereby enhanced the oil adsorption capacity. Several previous reports have reported that the adsorption of petroleum-based oil into graphene-based materials is mediated through van der Waals, electrostatic, π–π stacking, and hydrophobic interactions [58]. This result suggests that the oil adsorption on a sorbent material occurs through a physicochemical process [47,59,60].

Table 2
Comparison of kinetic and isotherm parameters of NR, NRG-0.5, and CM sorbent materials.

	NR	NGO-0.5	CM
$Q_{e,\exp}$ (g g^{-1})	9.47	16.80	6.58
Pseudo-first-order: $\ln(Q_e - Q_t) = \ln Q_e - k_1 t$			
$Q_{e,cal}$ (g g^{-1})	17.45	11.47	1.37
k_1 (s^{-1})	2.87	0.64	0.55
R^2	0.98	0.98	0.88
Pseudo-second-order: $\frac{t}{Q_t} = \frac{1}{k_2 Q_e^2} + \frac{1}{Q_e}$			
$Q_{e,cal}$ (g g^{-1})	9.87	17.42	6.97
k_2	0.47	0.52	0.45
R^2	0.99	0.99	0.99
Langmuir: $\frac{C_e}{Q_e} = \frac{1}{Q_m k_L} + \frac{C_e}{Q_m}$			
Q_m	9.80	16.80	6.22
R^2	0.99	0.99	0.99
k_L (L g^{-1})	36.52	37.30	14.09
R_L	0.05	0.05	0.12
Freundlich: $\ln Q_e = \ln k_F + \frac{1}{n} \ln C_e$			
n	7.74	7.94	1.09
k_F	12.51	18.33	5.32
R^2	0.60	0.70	0.89

Thus, the oil diffusion mechanisms of the sorbent materials were investigated by the intraparticle diffusion model. The relationships between Q_t and $t^{1/2}$ of the three sorbent materials are presented in Fig. 8. Each curve exhibited a linear plot of at least two but, most probably, three steps. We consider them to have three steps. In the first stage, the oil diffusion from the aqueous media to the sorbent surface or "surface diffusion" was evident and rapid. In the second stage, both intraparticle and pore diffusion occurred. The slope of the curve decreased and reached a rate-limiting step. In the final stage, the slope of each sorbent remained approximately constant, and the adsorption approached an equilibrium. The presence of rGO in the NR sorbent resulted in the highest diffusion rate (k_d) in all three stages and required the longest time to reach an equilibrium.

Based on the data, the oil diffusion mechanism is proposed in Fig. 9. When the crude oil was adsorbed by the sorbent surface, the oil dispersed widely and diffused into the sorbent surface.

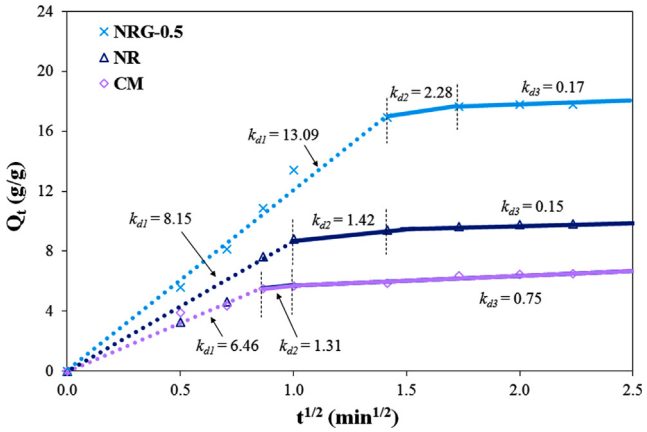

Fig. 8. Plot of intraparticle diffusion of crude-AXL oil adsorption of NR, NRG-0.5, and CM sorbent materials.

Afterward, the sorbent material swelled continuously until it reached an equilibrium. However, the maximal oil adsorption capacity was obtained for the NRG-0.5 sorbent because the NR network, its porosity, and the rGO particles enhanced the adsorption capacity. By contrast, the oil diffusion of the CM sample occurred only along the fibers. Hence, the oil was adsorbed inside the fibers, which resulted in a low oil adsorption capacity.

To study the maximal adsorption capacities of the sorbent materials, two isotherm models (Langmuir and Freundlich) were applied. The results are summarized in Table 2. The adsorption isotherm of each sorbent approximated the Langmuir isotherm with a correlation coefficient (R^2) of approximately 1 (0.99). The results imply that the adsorbed oil covered the entire cell surfaces of the materials with monolayer formations [16,47,61]. In addition, the maximal adsorption capacity (Q_m) of the sorbent materials approximated the experimental data ($Q_{e,exp}$). To clarify the adsorption preference of each sorbent material, the separation factor (R_L) was calculated. The results are listed in Table 2. The R_L values of the three sorbent materials varied between 0.05 and 0.12. Thus, crude AXL oil was preferred by each sorbent material. In addition, the R_L values of the NR and NRG-0.5 sorbents were 2.4 times lower than that of CM. Thus, the crude-oil adsorption behaviors of NR and NRG-0.5 were better than that of CM [47].

Recovery of sorbent materials

As well as the oil removal efficiency, the sorbent reusability is a crucial criterium in an oil spill cleanup. The reusability of sorbents minimizes the total amount of the waste generation for landfills and reduces the costs of oil spill removals. The oil recovery efficiencies of the NRG-0.5 and CM sorbents during 30 (NRG-0.5) or 15 (CM) successive adsorption–desorption cycles are presented in Fig. 10. The oil recovery of NRG-0.5 slightly decreased in the second to fourth cycle (to approximately 82%) because of the small amount of residual oil that was trapped inside the NR foam and foam pores after the swelling. After the fifth cycle, the adsorption capacity of NRG-0.5 saturated, which implies an oil removal of

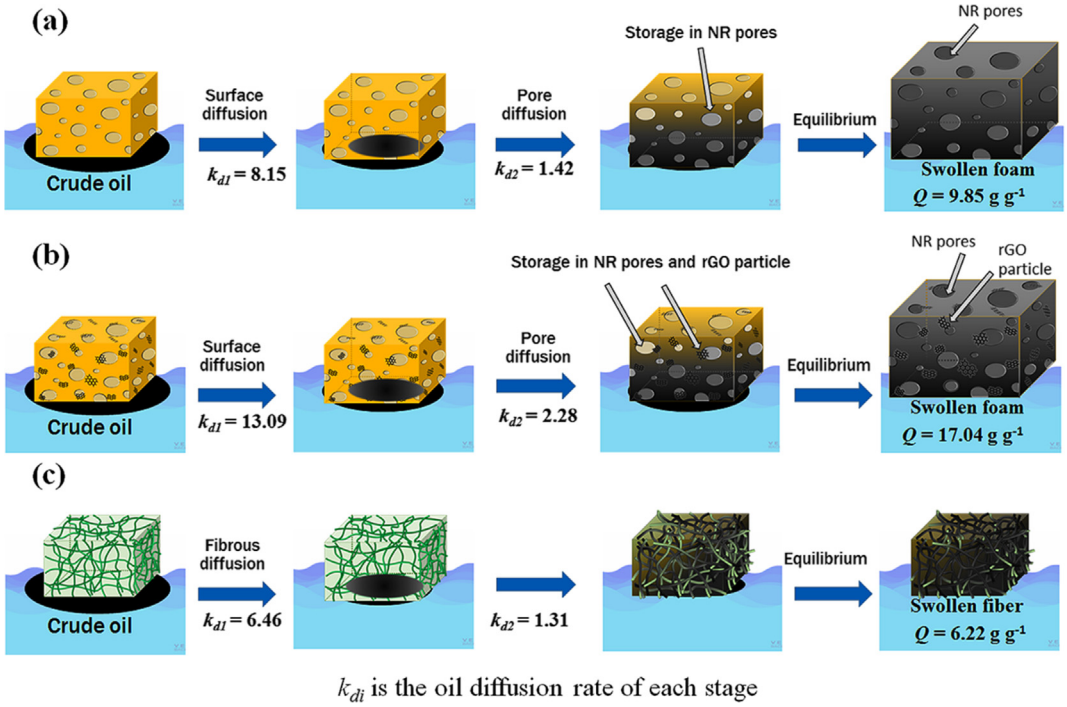

Fig. 9. Schematic of crude-AXL oil diffusion mechanisms of (a) NR, (b) NRG-0.5, and (c) CM sorbent materials.

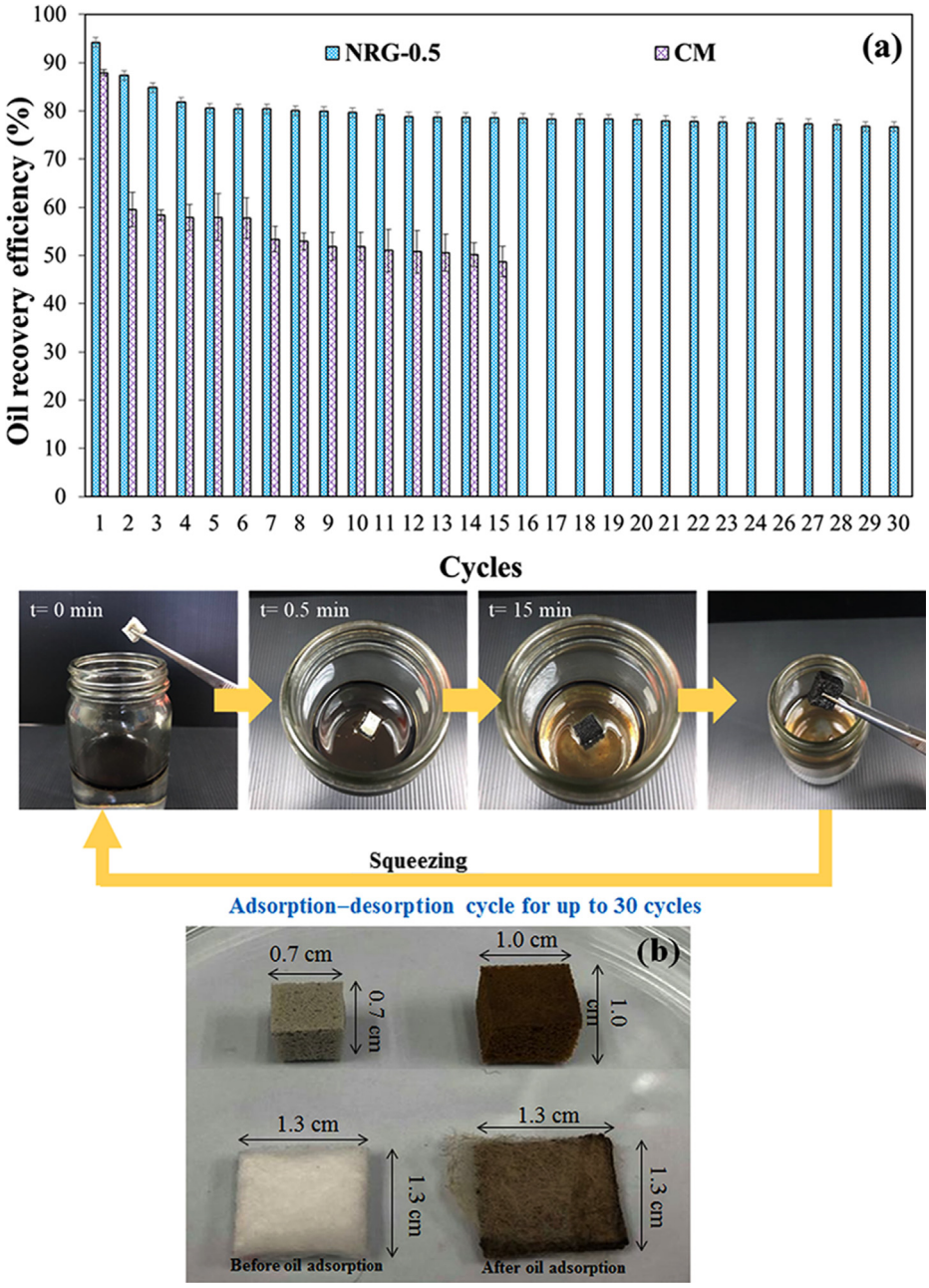

Fig. 10. (a) Oil removal efficiency for 30 (NRG-0.5) or 15 (CM) adsorption–desorption cycles and (b) physical characteristics of NRG-0.5 and CM sorbents before and after 30 (NRG-0.5) or 15 (CM) adsorption–desorption cycles.

more than 75% in each successive cycle. In addition, the NRG-0.5 foam exhibited no damages on the material surface, which expresses its good reusability.

By contrast, the oil removal ability of CM (32%) decreased remarkably after the first cycle and then slightly decreased with each subsequent reuse (up to 15 cycles) to <50%. Afterward, the surface was badly deteriorated, as shown in Fig. 9(b). Thus, no further adsorption–desorption cycles were performed. This result indicates that the good reusability of NRG-0.5 originates from the good elastic properties of the NR foam and the reinforcement effect of the rGO. In conclusion, this material can be applied as oil sorbent material to remove the leakage of oil in seawater.

The oil adsorption capacities of various oil sorbent materials are compared in Table 3. Various sorbent materials can be applied for the oil recovery in water. Additionally, several researchers suggest that the addition of a filler can enhance the oil adsorption capacity of sorbent foam including the present work. However, the oil adsorption capacity of each sorbent material depends on several factors such as the hydrophobic property of the sorbent material and the oil characteristics.

Conclusions

In this study, NRG composite foams were successfully prepared as petroleum oil sorbent material. The oil adsorption performances of the NRG sorbent materials depend on various factors, such as the morphology of the sorbent, rGO content, oil type, and oil properties. The high porosity of the NR foam in the presence of rGO enhances the oil adsorption capacity, which is optimal at 0.5 phr

Table 3
Comparison of oil adsorption capacities of various oil sorbent materials.

Sorbent	Oil type	Maximal oil adsorption ($g\ g^{-1}$)	Ref.
Graphene aerogel	Diesel oil	21.5	[62]
Graphene/PDMS[a]-coated sponge	Pump oil	95	[63]
Acetylated wheat straw	Diesel oil	24.2	[64]
MWrGO[b]/PDMS[a] composite	Pump oil	36.3	[27]
PUF[c]/nanoclay (3 wt%)	Crude oil	21.5	[65]
PUF[c]/lignin (10 wt%)	Crude oil	28.9	[16]
GN@PU[d]	Lubricating oil	31.0	[66]
NR	Crude oil	6–7	Present study
NRG-0.5	Crude oil	17–21	Present study

[a] Polydimethylsiloxane.
[b] Micro-wrinkled rGO.
[c] Polyurethane foam.
[d] Super-hydrophobic graphene-coated polyurethane.

rGO (NRG-0.5). Both NR foam and NRG-0.5 composite foam are more selective for gasoline than for crude AXL oil owing to the lower viscosity of the former, which enhances the oil diffusion into the sorbent materials. The NRG-0.5 composite exhibits the highest oil adsorption capacity for gasoline ($21.50\ g\ g^{-1}$) and crude AXL oil ($17.04\ g\ g^{-1}$). An increasing temperature of up to 45 °C or an external force (waves) increases the oil adsorption capacity of the sorbent material. The adsorption of crude AXL oil by the NR, NRG-0.5, and CM sorbents obeys the pseudo-second-order model, whereas the adsorption diffusion mechanism of the adsorption process is determined by the intraparticle diffusion model. The Langmuir isotherm is suitable for the experimental data. Thus, the crude-oil adsorption into the sorbents occurs as a mono-layer adsorption process. The high adsorption capacity of the NRG-0.5 sorbent for crude AXL oil is achieved through surface and pore diffusion through the NR network and rGO particles. By contrast, the oil diffusion mechanism of CM occurs only through fibrous diffusion. Most importantly, the high elasticity of NR and the presence of rGO in the NR composite foam improve the strength of the sorbent material. Thus, NRG-0.5 can be reused for at least 30 cycles without any damages. In conclusion, the NRG-0.5 composite foam presented in this study is a promising alternative oil sorbent for oil spill removals under critical field conditions in the ocean.

Acknowledgements

The financial support was provided by the International Postgraduate Program in Hazardous Substance and Environmental Management, Chulalongkorn University, and the Green Materials for Industrial Application Research Unit, Chulalongkorn University.

Conflict of interest

The authors have declared no conflict of interest.

Compliance with Ethics requirements

This article does not contain any studies with human or animal subjects.

References

[1] Zhu H, Qiu S, Jiang W, Wu D, Zhang C. Evaluation of electrospun polyvinyl chloride/polystyrene fibers as sorbent materials for oil spill cleanup. Environ Sci Technol 2011;45(10):4527–31.
[2] Elkady M, Hussien M, Abou-rady R. Equilibrium and kinetics behavior of oil spill process onto synthesized nano-activated carbon. Am J Appl Chem 2015;3(3–1):22–30.
[3] Yati I, Aydin GO, Sonmez HB. Cross-linked poly(tetrahydrofuran) as promising sorbent for organic solvent/oil spill. J Hazard Mater 2016;309:210–8.
[4] Ukotije-Ikwut PR, Idogun AK, Iriakuma CT, Aseminaso A, Obomanu T. A novel method for adsorption using human hair as a natural oil spill sorbent. Int J Sci Eng Res 2016;7:1754–65.
[5] Saleem J, Riaz MA, Gordon M. Oil sorbents from plastic wastes and polymers: a review. J Hazard Mater 2018;341:424–37.
[6] Pagnucco R, Phillips ML. Comparative effectiveness of natural by-products and synthetic sorbents in oil spill booms. J Environ Manage 2018;225:10–6.
[7] Shin JH, Heo J-H, Jeon S, Park JH, Kim S, Kang H-W. Bio-inspired hollow PDMS sponge for enhanced oil–water separation. J. Hazard. Mater. 2019;365:494–501.
[8] Al-Bahry S, Al-Wahaibi Y, Elshafie A, Al-Bemani A, Joshi S, Al-Makhmari H, et al. Biosurfactant production by *Bacillus subtilis* B20 using date molasses and its possible application in enhanced oil recovery. Int Biodeterior Biodegrad 2013;81:141–6.
[9] Liu J-F, Mbadinga S, Yang S-Z, Gu J-D, Mu B-Z. Chemical structure, property and potential applications of biosurfactants produced by *Bacillus subtilis* in petroleum recovery and spill mitigation. Int J Mol Sci 2015;16(3):4814–37.
[10] Rongsayamanont W, Soonglerdsongpha S, Khondee N, Pinyakong O, Tongcumpou C, Sabatini DA, et al. Formulation of crude oil spill dispersants based on the HLD concept and using a lipopeptide biosurfactant. J Hazard Mater 2017;334:168–77.
[11] Singh B, Bhattacharya A, Channashettar VA, Jeyaseelan CP, Gupta S, Sarma PM, et al. Biodegradation of oil spill by petroleum refineries using consortia of novel bacterial strains. Bull Environ Contam Toxicol 2012;89(2):257–62.
[12] Hussain I, Puschenreiter M, Gerhard S, Schöftner P, Yousaf S, Wang A, et al. Rhizoremediation of petroleum hydrocarbon-contaminated soils: improvement opportunities and field applications. Environ Exp Bot 2018;147:202–19.
[13] Guo M, Gong Z, Miao R, Rookes J, Cahill D, Zhuang J. Microbial mechanisms controlling the rhizosphere effect of ryegrass on degradation of polycyclic aromatic hydrocarbons in an aged-contaminated agricultural soil. Soil Biol Biochem 2017;113:130–42.
[14] Li B, Liu X, Zhang X, Zou J, Chai W, Lou Y. Rapid adsorption for oil using superhydrophobic and superoleophilic polyurethane sponge. J Chem Technol Biotechnol 2015;90(11):2106–12.
[15] Keshavarz A, Zilouei H, Abdolmaleki A, Asadinezhad A, Nikkhah A. Impregnation of polyurethane foam with activated carbon for enhancing oil removal from water. Int J Environ Sci Technol 2016;13(2):699–710.
[16] Santos O, da Silva MC, Silva V, Mussel W, Yoshida M. Polyurethane foam impregnated with lignin as a filler for the removal of crude oil from contaminated water. J Hazard Mater 2017;324:406–13.
[17] Carmody O, Frost R, Xi Y, Kokot S. Adsorption of hydrocarbons on organo-clays—implications for oil spill remediation. J Colloid Interface 2007;305(1):17–24.
[18] Karakasi O, Moutsatsou A. Surface modification of high calcium fly ash for its application in oil spill clean up. Fuel 2010;89(12):3966–70.
[19] Bandura L, Franus M, Józefaciuk G, Franus W. Synthetic zeolites from fly ash as effective mineral sorbents for land-based petroleum spills cleanup. Fuel 2015;147:100–7.
[20] Radetić MM, Jocić DM, Jovančić PM, Petrović ZL, Thomas HF. Recycled wool-based nonwoven material as an oil sorbent. Environ Sci Technol 2003;37(5):1008–12.
[21] Ali N, El-Harbawi M, Jabal AA, Yin C-Y. Characteristics and oil sorption effectiveness of kapok fibre, sugarcane bagasse and rice husks: oil removal suitability matrix. Environ Technol 2012;33(4):481–6.
[22] Singh V, Kendall RJ, Hake K, Ramkumar S. Crude oil sorption by raw cotton. Ind Eng Chem Res 2013;52(18):6277–81.
[23] Raj KG, Joy PA. Coconut shell based activated carbon–iron oxide magnetic nanocomposite for fast and efficient removal of oil spills. J Environ Chem Eng 2015;3(3):2068–75.
[24] Zhang A, Chen M, Du C, Guo H, Bai H, Li L. Poly(dimethylsiloxane) oil absorbent with a three-dimensionally interconnected porous structure and swellable skeleton. ACS Appl Mater Interfaces 2013;5(20):10201–6.
[25] Choi S-J, Kwon T-H, Im H, Moon D-I, Baek DJ, Seol M-L, et al. A polydimethylsiloxane (PDMS) sponge for the selective absorption of oil from water. ACS Appl Mater Interfaces 2011;3(12):4552–6.
[26] Tran DN, Kabiri S, Sim TR, Losic D. Selective adsorption of oil–water mixtures using polydimethylsiloxane (PDMS)–graphene sponges. Environ Sci: Water Res Technol 2015;1(3):298–305.
[27] Feng C, Yi Z, She F, Gao W, Zheng P, Garvey CJ, et al. Superhydrophobic and superoleophilic micro-wrinkled reduced graphene oxide as a highly portable and recyclable oil sorbent. ACS Appl Mater Interfaces 2016;8(15):9977–85.
[28] Zhang N, Zhong S, Chen T, Zhou Y, Jiang W. Emulsion-derived hierarchically porous polystyrene solid foam for oil removal from aqueous environment. RSC Adv 2017;7:22946–53.
[29] Yu S, Tan H, Wang J, Liu X, Zhou K. High porosity supermacroporous polystyrene materials with excellent oil–water separation and gas permeability properties. ACS Appl Mater Interfaces 2015;7:6745–53.
[30] Sethuraj MR, Mathew NT. Natural Rubber: Biology, Cultivation and Technology. Elsevier; 2012.

[31] Kohjiya S. Chemistry Manufacture and Applications of Natural Rubber. Elsevier; 2014.
[32] Ratcha A, Samart C, Yoosuk B, Sawada H, Reubroycharoen P, Kongparakul S. Polyisoprene modified poly (alkyl acrylate) foam as oil sorbent material. J Appl Polym Sci 2015;132:42688–97.
[33] Riyajan S, Keawittarit P. A novel natural rubber-graft-cassava starch foam for oil/gasohol absorption. Polym Int 2016;65:491–502.
[34] Venkatanarasimhan SA, Raghavachari D. Epoxidized natural rubber–magnetite nanocomposites for oil spill recovery. J Mater Chem A 2013;1:868–76.
[35] Li H, Liu L, Yang F. Covalent assembly of 3D graphene/polypyrrole foams for oil spill cleanup. J Mater Chem A 2013;1:3446–53.
[36] Zhang X, Liu D, Ma Y, Nie J, Sui G. Super-hydrophobic graphene coated polyurethane (GN@PU) sponge with great oil-water separation performance. Appl Surf Sci 2017;422:116–24.
[37] Wang Y, Wang B, Wang J, Ren Y, Xuan C, Liu C, et al. Superhydrophobic and superoleophilic porous reduced graphene oxide/polycarbonate monoliths for high-efficiency oil/water separation. J Hazard Mater 2018;344:849–56.
[38] Mukhopadhyay P, Gupta RK. Graphite, Graphene, and their Polymer Nanocomposites. CRC press; 2013.
[39] Zhang LL, Zhou R, Zhao XS. Graphene-based materials as supercapacitor electrodes. J Mater Chem 2010;20:5983–92.
[40] Wipatkrut P, Poompradub S. Exfoliation approach for preparing high conductive reduced graphite oxide and its application in natural rubber composites. Mater Sci Eng: B 2017;218:74–83.
[41] Pei S, Cheng HM. The reduction of graphene oxide. Carbon 2012;50:3210–28.
[42] Zhang J, Yang H, Shen G, Cheng P, Zhang J, Guo S. Reduction of graphene oxide via L-ascorbic acid. Chem Commun 2010;46:1112–4.
[43] ASTM F726-12: Standard Test Method for Sorbent Performance of Adsorbents, Annual Book of ASTM Standards, ASTM International: West Conshohocken; 2012.
[44] Lagergren S. Zur theorie der sogenannten adsorption geloster stoffe. K Sven Vetenskapsakad Hand 1898;24:1–39.
[45] Weber WJ, Morris JC. Kinetics of adsorption on carbon from solution. J Sanit Eng Div Am Soc Civil Eng 1963;89:31–60.
[46] Ho YS, McKay G. Pseudo-second order model for sorption processes. Process Biochem 1999;34:451–65.
[47] Hameed BH, Ahmad AA, Aziz N. Isotherms, kinetics and thermodynamics of acid dye adsorption on activated palm ash. Chem Eng J 2007;133:195–203.
[48] Langmuir I. The adsorption of gases on plane surfaces of glass, mica and platinum. J Am Chem Soc 1918;40:1361–403.
[49] Weber TW, Chakravorti RK. Pore and solid diffusion models for fixed-bed adsorbers. AICHE J 1974;20:228–38.
[50] Kumar R, Mehta BR, Bhatnagar M, Ravi S, Mahapatra S, Salkalachen S, Jhawar P. Graphene as a transparent conducting and surface field layer in planar Si solar cells. Nanoscale Res Lett 2014;9:1–9.
[51] Zhan Y, Wan X, He S, Yang Q, He Y. Design of durable and efficient poly(arylene ether nitrile)/bioinspired polydopamine coated graphene oxide nanofibrous composite membrane for anionic dyes separation. Chem Eng J 2018;333:132–45.
[52] Ni Z, Wang Y, Yu T, Shen Z. Raman spectroscopy and imaging of graphene. Nano Res 2008;1:273–91.
[53] Younker JM, Walsh ME. Impact of salinity and dispersed oil on adsorption of dissolved aromatic hydrocarbons by activated carbon and organoclay. J Hazard Mater 2015;299:562–9.
[54] Duong HTT, Burford RP. Effect of foam density, oil viscosity, and temperature on oil sorption behavior of polyurethane. J Appl Polym Sci 2006;99:360–7.
[55] Chen N, Pan Q. Versatile fabrication of ultralight magnetic foams and application for oil–water separation. ACS Nano 2013;7:6875–83.
[56] Amin JS, Abkenar MV, Zendehboudi S. Natural sorbent for oil spill cleanup from water surface: environmental implication. Ind Eng Chem Res 2015;54:10615–21.
[57] Shiu RF, Lee CL, Hsieh PY, Chen CS, Kang YY, Chin WC, et al. Superhydrophobic graphene-based sponge as a novel sorbent for crude oil removal under various environmental conditions. Chemosphere 2018;207:110–7.
[58] Wang X, Liu B, Lu Q, Qu Q. Graphene-based materials: fabrication and application for adsorption in analytical chemistry. J Chromatogr A 2014;1362:1–15.
[59] Ho YS, McKay G. The kinetics of sorption of basic dyes from aqueous solution by sphagnum moss peat. Can J Chem Eng 1998;76:822–7.
[60] Tan IAW, Ahmad AL, Hameed BH. Adsorption isotherms, kinetics, thermodynamics and desorption studies of 2, 4, 6-trichlorophenol on oil palm empty fruit bunch-based activated carbon. J Hazard Mater 2009;164:473–82.
[61] Shahbazi A, Younesi H, Badiei A. Functionalized SBA-15 mesoporous silica by melamine-based dendrimer amines for adsorptive characteristics of Pb (II), Cu (II) and Cd (II) heavy metal ions in batch and fixed bed column. Chem Eng J 2011;168:505–18.
[62] Huang J, Yan Z. Adsorption mechanism of oil by resilient graphene aerogels from oil-water emulsion. Langmuir 2018;34(5):1890–8.
[63] Nguyen DD, Tai NH, Lee SB, Kuo WS. Superhydrophobic and superoleophilic properties of graphene-based sponges fabricated using a facile dip coating method. Energy Environ Sci 2012;5:7908–12.
[64] Lv E, Xia W, Tang M, Pu Y. Preparation of an efficient oil-spill adsorbent based on wheat straw. BioResources 2017;12(1):296–315.
[65] Nikkhah AA, Zilouei H, Asadinezhad A, Keshavarz A. Removal of oil from water using polyurethane foam modified with nanoclay. Chem Eng J 2015;2015 (262):278–85.
[66] Zhang X, Liu D, Ma Y, Nie J, Sui G. Super-hydrophobic graphene coated polyurethane (GN@ PU) sponge with great oil-water separation performance. Appl Surf Sci 2017;422:116–24.